We are IntechOpen, the world's leading publisher of Open Access books Built by scientists, for scientists

4,800
Open access books available

122,000
International authors and editors

135M
Downloads

Our authors are among the

154
Countries delivered to

TOP 1%
most cited scientists

12.2%
Contributors from top 500 universities

CLARIVATE ANALYTICS BOOK CITATION INDEX INDEXED

WEB OF SCIENCE™

Selection of our books indexed in the Book Citation Index in Web of Science™ Core Collection (BKCI)

Interested in publishing with us?
Contact book.department@intechopen.com

Numbers displayed above are based on latest data collected.
For more information visit www.intechopen.com

8

Fabrication and Study on One-Transistor-Capacitor Structure of Nonvolatile Random Access Memory TFT Devices Using Ferroelectric Gated Oxide Film

Chien-Min Cheng, Kai-Huang Chen, Chun-Cheng Lin,
Ying-Chung Chen, Chih-Sheng Chen and Ping-Kuan Chang
Department of Electronics Engineering, Tung-Fang Design University,
Department of Electronic Engineering, Southern Taiwan University,
Department of Mathematics and Physics, Chinese Air Force Academy,
R.O.C.

1. Introduction

Recently, non-volatile and volatile memory devices such as static random access memory (SRAM), dynamic random access memory (DRAM), Flash memory, EPROM and E^2PROM were very important for applications in conventional personal computer and micro-processor, and performance efficiency of hardware improved by their low voltage, high operation speed, and large storage capacity. The non-volatile memory devices were widely investigated and discussed among these memory devices. Many kind of the non-volatile memory device were ferroelectric random access memory (FeRAM), magnetron random access memory (MRAM), and resist random access memory (RRAM) devices. Up to now, the non-volatile ferroelectric random access memory (FeRAM) devices were attractive because of their low coercive filed, large remnant polarization, and high operation speed among various non-volatile access random memory devices [1].

The non-volatile FeRAM devices were limited by their relative larger one-transistor-one-capacitor (1T-1C) size. Thus, one-transistor-capacitor (1TC) structure ferroelectric memory was desirable because of the better sensitivity and small size than 1T-1C structure ferroelectric memory [2-4]. The operation characteristics and reliability of ferroelectric capacitor structure of 1T-1C memory cell were spending lots cost during the fabrication process.

In addition, electronic devices and system-on-panel (SOP) technology were widely discussed and researched. For SOP concept, the switch characteristics of various thin-film transistor (TFT) structures were widely investigated for applications in amorphous silicon (α-Si) and polycrystal silicon (poly-Si) active matrix liquid-crystal-display (AM-LCD) displays [5-7]. Integrated electron devices such as memory devices, control devices, and central processing units (CPU) on transparent conductive thin films will be important in the future. The excellent electrical, physical, and reliability characteristics of metal-ferroelectric-metal (MFM) capacitor structures for 1T1C memory cells were enhanced using transparent conductive thin films on glass substrates.

2. Electrical properties of non-volatile RAM using ferroelectric thin film

S. Y. Wu firstly reported that an MFS transistor fabricated by using bismuth titanate in 1974 [2-3]. The first ferroelectric memory device was fabricated by replacing the gate oxide of a conventional metal-oxide-semiconductor (MOS) transistor with a ferroelectric material. However, the interface and interaction problem between the silicon substrate and ferroelectric films were very important factors during the high temperature processes in 1TC structure. To overcome the interface and interaction problem, the silicon dioxide and silicon nitride films were used as the buffer layer. The low remnant polarization and high operation voltage of 1TC were also be induced by gate oxide structure with double-layer ferroelectric silicon dioxide thin films. Sugibuchi et al. provided a 50 nm silicon dioxide thin film between the $Bi_4Ti_3O_{12}$ layer and the silicon substrate [8].

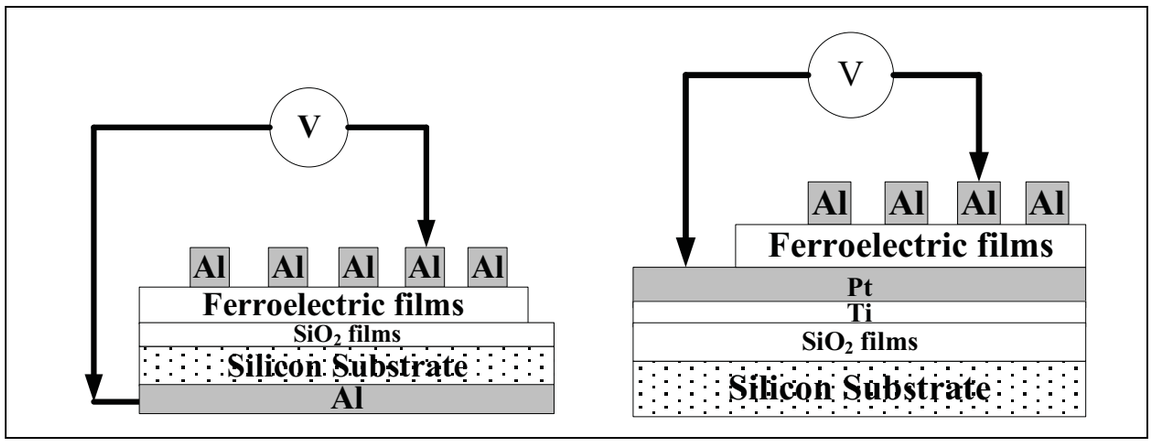

Fig. 1. (a) Metal-ferroelectric-insulator-semiconductor (MFIS) structure, and (b) Metal ferroelectric-metal (MFM) structure.

The ferroelectric ceramic target prepared, the raw materials were mixed and fabricated by solid state reaction method. After mixing and ball-milling, the mixture was dried, grounded, and calcined for some time. Then, the pressed ferroelectric ceramic target with a diameter of two inches was sintered in ambient air. The base pressure of the deposited chamber was brought down 1×10^{-7} mTorr prior to deposition. The target was placed away from the $Pt/Ti/SiO_2/Si$ and SiO_2/Si substrate. For metal-ferroelectric-metal (MFM) capacitor structure, the Pt and the Ti were deposited by dc sputtering using pure argon plasma as bottom electrodes. The SiO_2 thin films were prepared by dry oxidation technology. The metal-ferroelectric-insulator-semiconductor (MFIS) and metal-ferroelectric-metal (MFM) structures were shown in Fig. 1.

For the physical properties of ferroelectric thin films obtained, the thickness and surface morphology of ferroelectric thin films were observed by field effect scanning electron microscopy (FeSEM). The crystal structure of ferroelectric thin films were characterized by an X-ray diffraction (XRD) measurement using a Ni-filtered CuKα radiation. The capacitance-voltage (C-V) properties were measured as a function of applied voltage by using a Hewlett-Packard (HP 4284A) impedance gain phase analyzer. The current curves versus the applied voltage (I-V characteristics) of the ferroelectric thin films were measured by a Hewlett-Packard (HP 4156) semiconductor parameter analyzer.

Additionally, the ferroelectric thin films were used in a one-transistor-capacitor (1TC) structure of the amorphous-Si TFT device to replace the gate oxide of random access memory devices. For that, a bottom-gate amorphous thin-film transistor, as shown in Fig.2, would be fabricated and the characteristics of the fabricated devices were successfully developed.

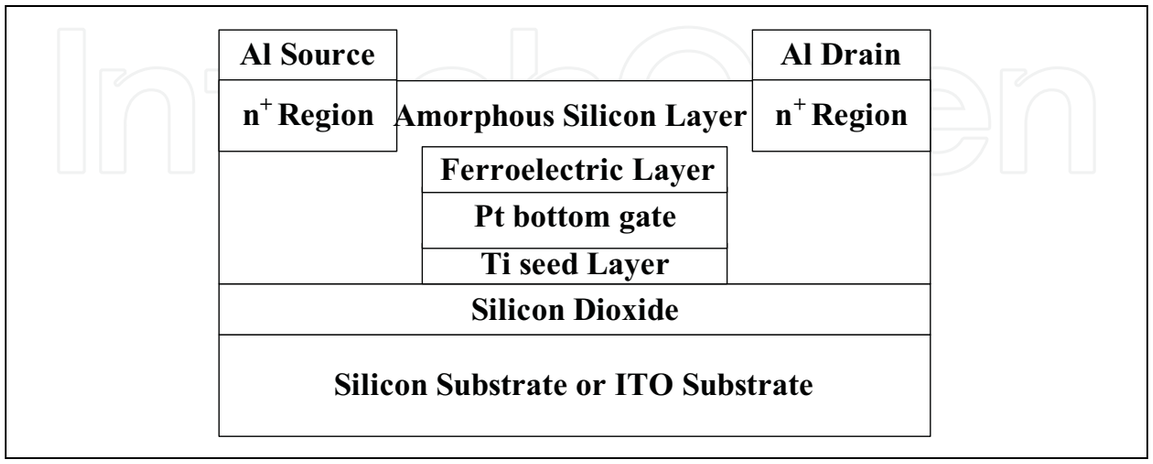

Fig. 2. The 1TC FeRAM device fabricated with ferroelectric thin film.

For 1TC FeRAM device fabricated, a one-transistor-capacitor (1TC) structure of the amorphous-Si (a-Si) TFT device was designed and fabricated. In Fig. 2, the a-Si TFT were fabricated by depositing ferroelectric ferroelectric thin films gate oxide on bottom gate Pt/Ti/SiO_2/Si substrate. A silicon oxide film, acting as a buffer oxide, was deposited on gate oxide substrate by plasma enhanced chemical vapor deposition (PECVD). A amorphous silicon film, acting as an active channel, was also deposited by PECVD method. Additionally, the source and drain regions were doped phosphorous by an ion implantation method. A aluminum films was deposited as the source and drain electrodes.

Finally, the a-Si TFT was heat treated for 1h in N_2 ambient for the purpose of alloying. The a-Si TFT with the dimensions of 40 μm in width and 8 μm in length were designed and fabricated and the I_D-V_G transfer characteristics of 1TC FeRAM devices were measured. The operation characteristic of 1TC structure for TFT devices was similar to SONOS structure of non-volatile flash memory device.

2.1 ABO_3 and $BLSF_s$ structure material

The (ABO_3) pervoskite and bismuth layer structured ferroelectrics (BLSFs) were excellent candidate materials for ferroelectric random access memories (FeRAMs) such as in smart cards and portable electric devices utilizing their low electric consumption, nonvolatility, high speed readout. The ABO_3 structure materials for ferroelectric oxide exhibit high remnant polarization and low coercive filed. Such as Pb(Zr,Ti)O_3 (PZT), $Sr_2Bi_2Ta_2O_9$ (SBT), $SrTiO_3$ (ST), Ba(Zr,Ti)O_3 (BZ1T9), and (Ba,Sr)TiO_3 (BST) were widely studied and discussed for large storage capacity FeRAM devices. The (Ba,Sr)TiO_3 and Ba(Ti,Zr)O_3 ferroelectric materials were also expected to substitute the PZT or SBT memory materials and improve the environmental pollution because of their low pollution problem [9-15]. In addition, the

high dielectric constant and low leakage current density of zirconium and strontium-doped $BaTiO_3$ thin films were applied for the further application in the high density dynamic random access memory (DRAM) [16-20].

2.1.1 ABO3 pervoskite structure material system

For ABO_3 pervoskite structure such as, $BaTiO_3$ and BZ1T9, the excellent electrical and ferroelectric properties were obtained and found. For SOP concept, the ferroelectric BZ1T9 thin film on ITO substrate were investigated and discussed. For crystallization and grain grow of ferroelectric thin films, the crystal orientation and preferred phase of different substrates were important factors for ferroelectric thin films of MIM structures. The XRD patterns of BZ1T9 thin films with 40% oxygen concentration on $Pt/Ti/SiO_2/Si$ substrates from our previous study were shown in Fig. 3 [21-22]. The (111) and (011) peaks of the BZ1T9 thin films on $Pt/Ti/SiO_2/Si$ substrates were compared with those on ITO substrates. The strongest and sharpest peak was observed along the Pt(111) crystal plane. This suggests that the BZ1T9 films grew epitaxially with the Pt(111) bottom electrode. However, the (111) peaks of BZ1T9 thin films were not observed for (400) and (440) ITO substrates. Therefore, we determined that the crystallinity and deposition rate of BZ1T9 thin films on ITO substrates differed from those in these study [21-24].

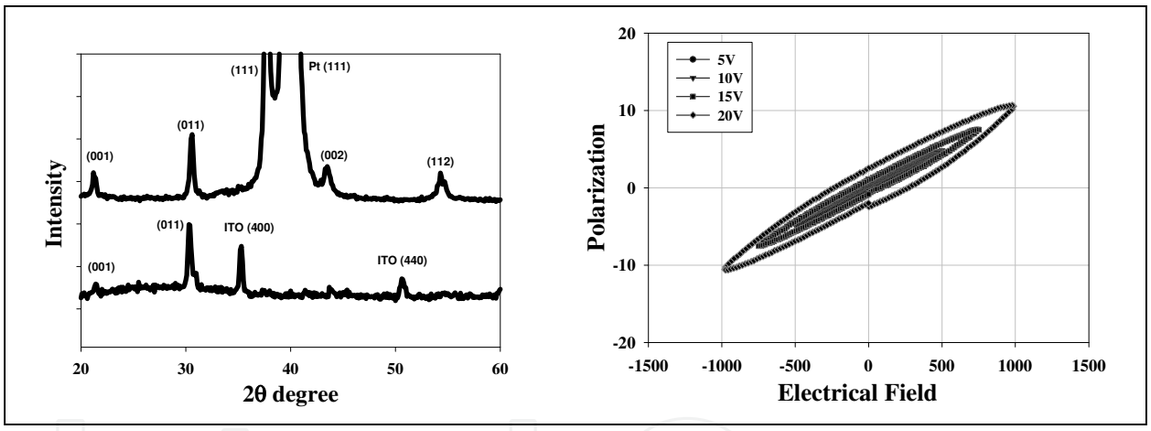

Fig. 3. (a) XRD patterns of as-deposited thin films on the ITO/glass and Pt substrates, and (b) P-E curves of thin films.

The polarization versus applied electrical field (P-E) curves of as-deposited BZ1T9 thin films were shown in Fig. 3(a). As the applied voltage increases, the remanent polarization of thin films increases from 0.5 to 2.5 $\mu C/cm^2$. In addition, the $2P_r$ and coercive field calculated and were about 5 $\mu C/cm^2$ and 250 kV/cm, respectively. According to our previous study, the BZ1T9 thin film deposited at high temperature exhibited high dielectric constant and high leakage current density because of its polycrystalline structure [21].

2.1.2 Bismuth layer ferroelectric structure material system

Bismuth titanate system based materials were an important role for FeRAMs applications. The bismuth titanate system were given in a general formula of bismuth layer structure ferroelectric, $(Bi_2O_2)^{2+}(A_{n-1}B_nO_{3n+1})^{2-}$ (A=Bi, B=Ti). The high leakage current, high dielectric loss

and domain pinning of bismuth titanate system based materials were caused by defects, bismuth vacancies and oxygen vacancies. These defects and oxygen vacancies were attributed from the volatilization of Bi_2O_3 of bismuth contents at elevated temperature [25-27].

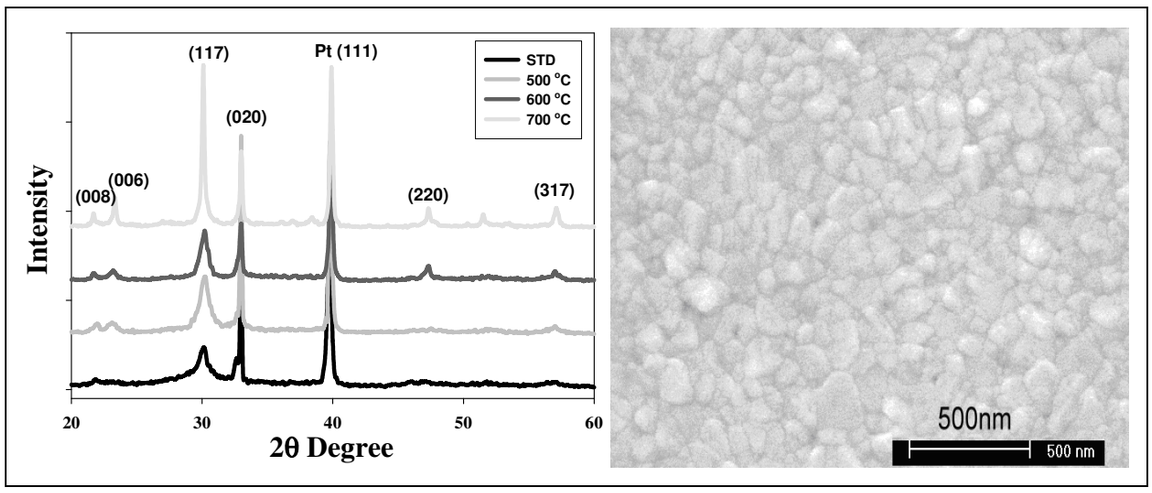

Fig. 4. (a) XRD patterns of as-deposited $Bi_4Ti_3O_{12}$ thin films, and (b)The SEM morphology of as-deposited $Bi_4Ti_3O_{12}$ films.

The XRD patterns of as-deposited $Bi_4Ti_3O_{12}$ thin films and ferroelectric thin films under 500~700°C rapid thermal annealing (RTA) process were compared in Fig. 4. From the results obtained, the (002) and (117) peaks of as-deposited $Bi_4Ti_3O_{12}$ thin film under the optimal sputtering parameters were found. The strong intensity of XRD peaks of $Bi_4Ti_3O_{12}$ thin film under the 700°C RTA post-treatment were be found. They were (008), (006), (020) and (117) peaks, respectively. Compared the XRD patterns shown in Fig. 4, the crystalline intensity of (111) plane has no apparent increase as the as-deposited process is used and has apparent increase as the RTA-treated process was used. And a smaller full width at half maximum value (FWHM) is revealed in the RTA-treated $Bi_4Ti_3O_{12}$ thin films under the 700°C post-treatment. This result suggests that crystal structure of $Bi_4Ti_3O_{12}$ thin films were improved in RTA-treated process.

The surface morphology observations of as-deposited $Bi_4Ti_3O_{12}$ thin films under the 700°C RTA processes were shown in Fig. 4. For the as-deposited $Bi_4Ti_3O_{12}$ thin films, the morphology reveals a smooth surface and the grain growth were not observed. The grain size and boundary of $Bi_4Ti_3O_{12}$ thin films increased while the annealing temperature increased to 700°C. In RTA annealed $Bi_4Ti_3O_{12}$ thin films, the maximum grain size were about 200 nm and the average grain size is 100 nm. As shown in Fig. 4, the thickness of annealed $Bi_4Ti_3O_{12}$ thin films were calculated and found from the SEM cross-section images. The thickness of the deposited $Bi_4Ti_3O_{12}$ thin films is about 800 nm and the deposited rate of $Bi_4Ti_3O_{12}$ thin films is about 14 nm/mim.

2.1.3 The influence of doping effect on the electrical properties of ferroelectric films

In the past, we found that using V_2O_5 as the addition or substitution would improve the dielectric characteristics of $SrBi_2Ta_2O_9$ ceramics [28]. Vanadium doped $Bi_4Ti_3O_{12}$ thin films were also found to have very large remanent polarization (2Pr) and the coercive field (Ec).

But the leakage current density, the memory window and the changing ratio of memory window of vanadium doped $Bi_4Ti_3O_{12}$ thin films measured using the MFIS structure were not developed before [29-31].

Figure 5(a) shows ferroelectric hysteresis loops of $Bi_4Ti_3O_{12}$ and as-deposited BTV thin film capacitors measured with a ferroelectric tester (Radiant Technologies RT66A). The as-deposited BTV thin films clearly show ferroelectricity characteristics. The remanent polarization and coercive field were 23 μC/cm² and 450 kV/cm. To compare the vanadium doped and undoped $Bi_4Ti_3O_{12}$ thin films, the remanent polarization (2Pr) were increased form 16μC/cm² for undoped $Bi_4Ti_3O_{12}$ thin films to 23 μC/cm² for vanadium doped. However, the coercive field of as-deposited BTV thin films would be increased to 450 kV/cm. These results indicated that the substitution of vanadium was effective for the appearance of ferroelectricity at 550 °C. The 2Pr value and the Ec value were larger than those reported in Refs. [9-10], and the 2Pr value was smaller and the Ec value was larger than those reported in [31]. Based on above results, it was found that the simultaneous substitutions for B-site are effective to derive enough ferroelectricity by accelerating the domain nucleation and pinning relaxation caused by B-site substitution [32-35].

Figure 5(b) shows the C-V curves of as-deposited vanadium doped BTV and un-doped BIT thin films. The applied voltages, which are first changed from -20 to 20 V and then returned to -20 V, are used to measure the capacitance voltage characteristics (C-V) of the MFIS structures. For the vanadium doped thin films, the memory window of MFIS structure increased from 5 to 15 V, and the threshold voltage decreased from 7 to 3 V. This result demonstrated that the lower threshold voltage and decreased oxygen vacancy in undoped BIT thin films were improved from the C-V curves measured.

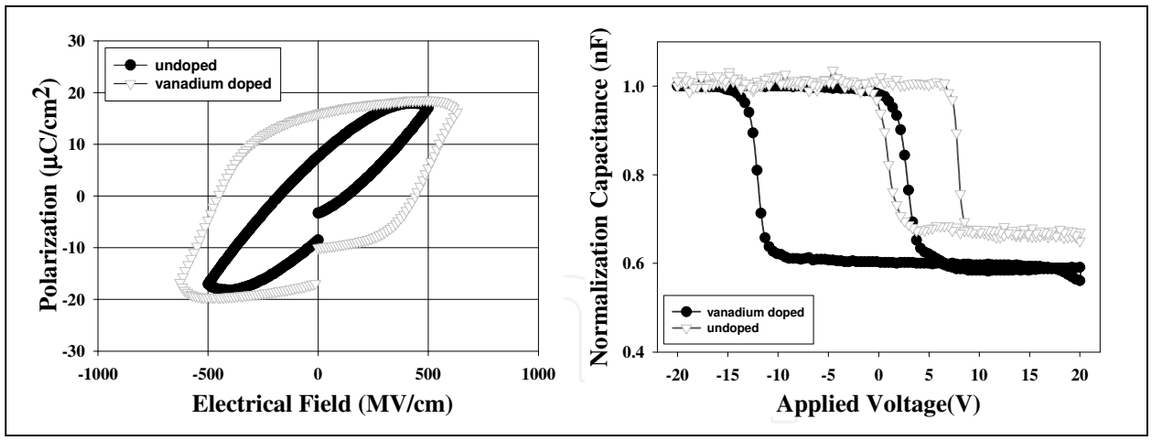

Fig. 5. (a) The P-E characteristics of vanadium doped and undoped thin films, and (b) The normalization C-V curves of vanadium doped and undoped thin films.

According to pervious study, the $Bi_4Ti_3O_{12}$ materials exhibit high leakage current and domain pinning properties because of the defects such as bismuth and oxygen vacancies. The BTV thin film was prepared by substituting a bismuth ion with a lanthanum ion at A-site substitution, and the fatigue endurance characteristics was improved [36]. In addition, the B-site substitution by high-valent cation was mainly the compensation for the defects. These defects caused by the fatigue phenomenon and strong domain pinning [37-40].

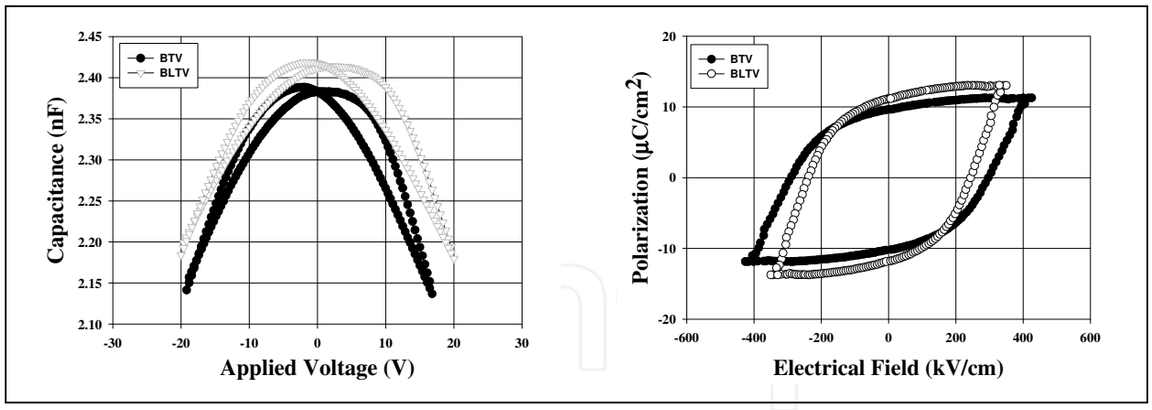

Fig. 6. (a) The C-V characteristics of as-deposited BTV and BLTV thin films, and (b) The P-E characteristics of as-deposited BTV and BLTV thin films.

Figure 6(a) shows the change in the C-V curves of the BTV and BLTV thin films in MFM structure measured at 100 kHz. The applied voltages, which were first changed from -20 to 20 V and then returned to -20 V, were used to measure the capacitance voltage characteristics (C-V). The BLTV thin films exhibited high capacitance than those of BTV thin films. We found that the capacitances of the lanthanum-doped BTV thin films were increased.

Figure 6(b) shows the P-E curves of the different ferroelectric thin films under applied voltage of 18V from the Sawyer–Tower circuits. The remanent polarization of non-doped, vanadium-doped, and lanthanum-doped ferroelectric thin films linearly was increased from 5, 10 to 11 μC/cm², respectively. The coercive filed of non-doped, vanadium-doped, and lanthanum-doped ferroelectric thin films were about 300, 300, and 250 kV/cm, respectively. The ferroelectric properties of lanthanum-doped and vanadium-doped BIT thin films were improved and found.

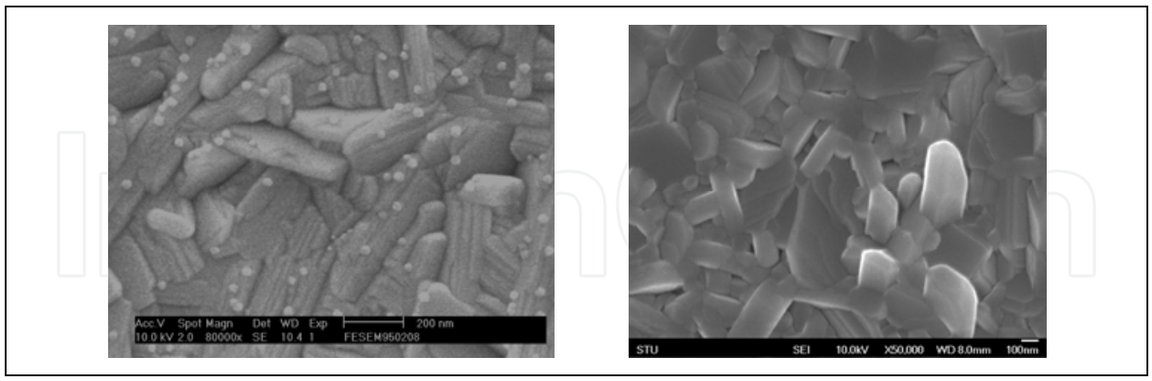

Fig. 7. The surface morphology of as-deposited BTV and BLTV thin films.

In Fig. 7, rod-like and circular-board grains were observed with scanning electron microscopy (SEM) for as-deposited BTV films. The small grain was gold element in preparation for the SEM sample. However, the BLTV thin films exhibited a great quantity rod-like grain structure in Fig. 7. The rod-like grain size of BLTV thin films was larger than those of BTV. We induced that the bismuth vacancies of BTV thin films compensate for lanthanum addition and micro-structure were improved in BLTV thin films.

2.2 Improved properties for ferroelectric films using post-treatment technology

The electrical and physical characteristics were affected by defect and oxygen vacancy of grain boundary in various oxide materials for applications in electrical integrated circuits. The defects and oxygen vacancies in conventional oxide films were usually filled and compensated by oxygen gas using different deposition methods in the semiconductor manufacturing process. The crystal structure of the various oxide films was improved by the high deposition temperature. However, the oxygen elements in grain boundary of the thin films were broken and lost above the deposition temperatures of 550°C [41–47]. To improve the properties of various oxide materials under the post-treatment process, the conventional temperature annealing (CTA) and rapid thermal annealing (RTA) processing were sometimes essential and indispensable technology for crystallization and quality of thin films [48-52].

2.2.1 CFA and RTA post-treatment technology

Ferroelectric thin films prepared by rapid temperature annealing (RTA) and conventional temperature annealing (CFA) processing were reported extensively. Many studies had been reported that rapid temperature annealing method was successfully to increase the electrical and physical properties [53-56]. In addition, grain size, electrical properties and surface roughness are greatly affected by annealing temperature under conventional furnace annealing.

To study the characteristics of thin films of perovskite oxide BZ1T9, deposited on ITO glass substrate using the different RTA annealing temperatures were found. In which, the characteristics of the Al/BZ1T9/ITO glass (MFM) structures, were reported and the relationship between the electrical properties and different annealing temperature of MFM structure was investigated. In addition, preferred orientation, crystal phase and dielectric properties of BZ1T9 thin films by different annealing temperatures were discussion and evaluated.

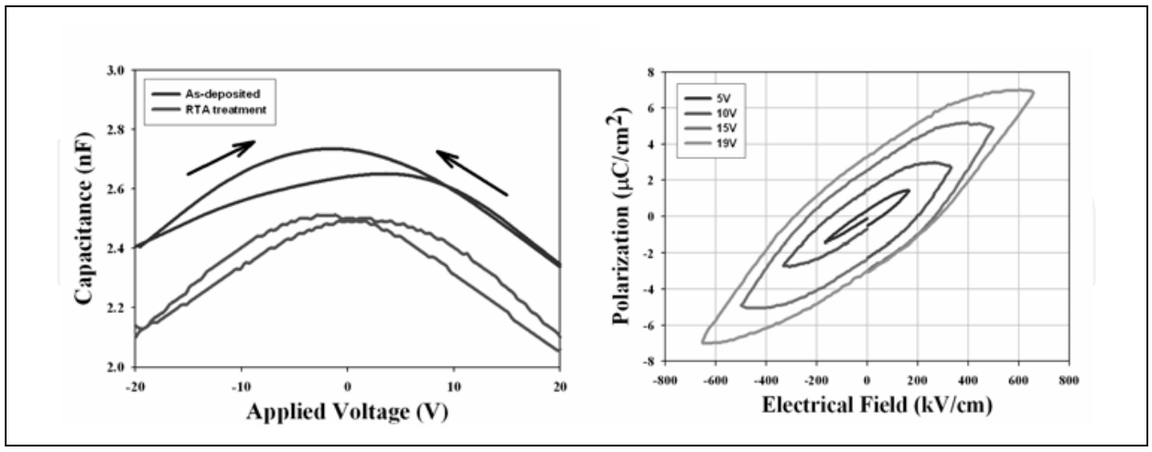

Fig. 8. (a) The C-V characteristics of as-deposited and RTA-treated thin films, and (b) The P-E characteristics of RTA-treated thin films.

Figure 8(a) shows the C-V curves of as-deposited and annealed BZ1T9 films when applied voltage of ±20V. From the experiments obtained, the capacitance of RTA annealed BZ1T9 films increased while the temperature increased to 650°C. Besides, the maximum dielectric

constant of RTA annealed BZ1T9 films were found. In addition, the larger grain size of annealed BZ1T9 films were attributed to this reason.

The leakage current density versus applied electrical field (J-E) curves of as-deposited BZ1T9 films under 650°C RTA process were also found. The leakage current densities of as-deposited BZ1T9 films using RTA process were about 2×10^{-6} A/cm^2 under the electrical field of 0.5 MV/cm. It showed that the leakage current density of annealed-BZ1T9 films was larger than those of as-deposited BZ1T9.

The P-E curves of as-deposited BZ1T9 thin films at a frequency of 100 kHz was shown in Fig. 8(b). As the applied voltage increases, the remanent polarization of thin films increases. In addition, the $2P_r$ and coercive field are also calculated and were about 6 μC/cm^2 and 250 kV/cm, respectively. According to our previous study, the BZ1T9 thin film deposited at a higher temperature exhibits a higher dielectric constant and a higher leakage current density because of its polycrystalline structure [57].

2.2.2 Oxygen plasma post-treatment technology

The high-temperature process for integrated fabrication on electronic devices was a serious problem. The gas-like and excellent properties of the oxygen plasma process were attracted considerable research in efficiently transporting oxygen atom and nodamaging diffusion into the microstructures of oxide materials at a low-temperature treatment. Decreased and passivated the traps and defects of oxide materials were the most advantages.

Figure 9(a) shows the leakage current density versus electrical filed (J-E) curves of as-deposited BSTZ thin films treated as a function of oxygen plasma treatment times. The leakage current density of BSTZ thin films was decreased as oxygen plasma treatment times increased. The leakage current density of treated thin films was lower than those of as-deposited thin films. We also found that the leakage current density of the BSTZ thin films for 3 minutes plasma treatment time were similar to those for 6-9 minutes plasma treatment time. To discuss the defects and oxygen vacancies effect, the leakage current versus electrical field curves were fitted to the Schottky emission and Poole-Frankel transport models [58–60]. The fitting curve was straight line, and the J–E curves of as-deposited thin films after oxygen plasma treatment obey the Schottky emission model in fig. 2. From the experimental results, the low leakage current density of plasma treated thin films was attributed to less oxygen defects and vacancies.

Figure 8(b) shows the capacitances-voltage (C-V) curves of non-treatment and oxygen plasma treatment BSTZ thin films. The capacitance of thin films was increased while the oxygen treatment time increased. The capacitance of thin films was increased. As the results, the improvement of capacitance of BSTZ thin films were attributed to the oxygen ion vacancy compensated.

In addition, we found that the wide-scan XPS spectrum of the as-deposited thin film for oxygen plasma treatment in the binding energy range from 100 to 1keV. From the XPS spectrum, it revealed that the thin films contained Ba 3d, Sr 3d, Ti 2p, Zr 3d, and O 1s elements. After oxygen plasma treated, the LBE and HBE were increased to 533.6 and 535.8 eV. These results induced that the oxygen plasma operatively react with the dangling bonds of thin films and form the stronger O 1s bonding. The O 1s binding energy of the BSTZ thin film after oxygen plasma treatment was increased.

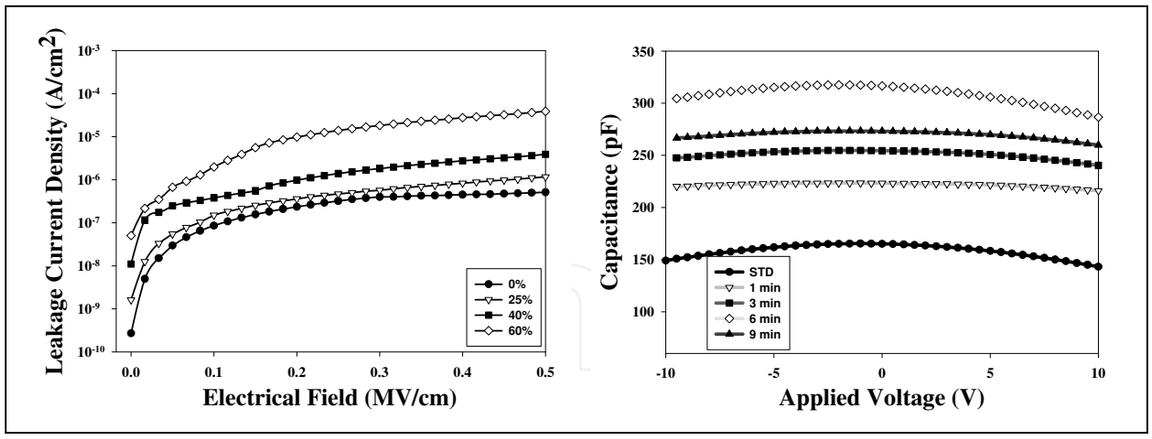

Fig. 9. (a) The J-E characteristics of as-deposited and plasma-treated BSTZ thin films, and (b) The C-V characteristics of as-deposited and plasma-treated BSTZ thin films.

For other ferroelectric thin film, the leakage current density versus applied voltage (J-E) curves of the BZ1T9 thin films was shown in Fig. 5. At an electric field of 0.25 MV/cm, the oxygen-plasma-treated films exhibit a leakage current density two orders of magnitude lower than those of the non-oxygen-plasma-treated ones. As mentioned above, the oxygen plasma treatment decreases the oxygen vacancies and the leakage current density.The current-field curves were fit to Schottky emission and Poole-Frankel transport models to determine whether the observed decrease in leakage current of the oxygen plasma treated films [58-60]. Smyth et al. reported that oxygen escapes during thermal process, and the oxygen vacancies are subsequently generated according to O_o <-> V_o^{++} + 2e- + 1/2 O_2, that the O_o, V_o^{++}, and e- denote the oxygen ion at its normal site, oxygen vacancy, and electron, respectively. For that, a lot of oxygen vacancies will exist after 9 min the oxygen plasma treatment.

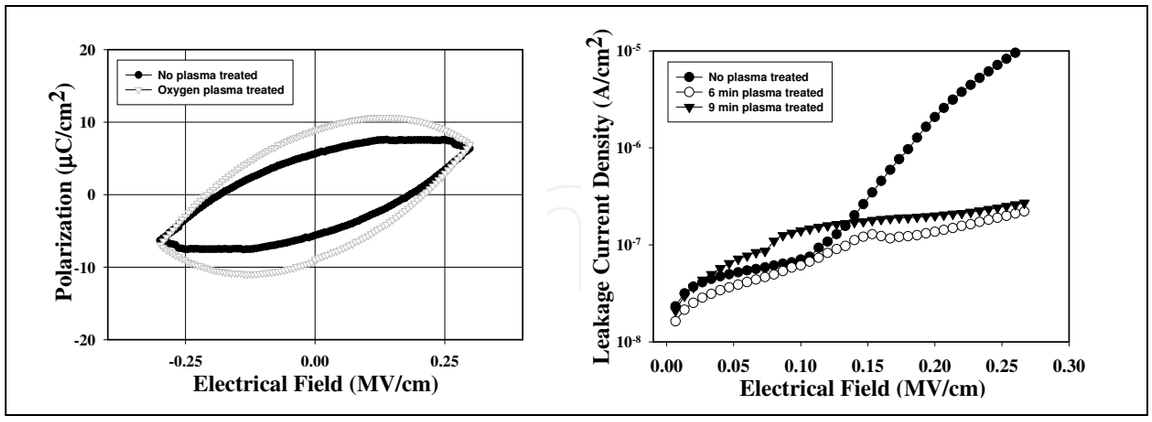

Fig. 10. (a) The P-E characteristics of as-deposited and plasma-treated BZ1T9 thin films, and (b) The J-E characteristics of as-deposited and plasma-treated BZ1T9 thin films.

Figure 10(a) shows the P-E curves of the BZ1T9 films observed at a frequency of 100 kHz under an applied electrical field of 0–0.28 MV/cm from the Sawyer-Tower circuits. After oxygen plasma treatment, the coercive field does not appear to change; however, the remnant polarization appears to increase from 6 to 9 μC/cm2. As shown in Fig. 10(b), we

observed that the saturation polarization decreases slightly when an electrical field of 280 kV/cm was applied. This effect can be caused by the high leakage current density under stronger electrical fields.

2.2.3 Supercritical carbon dioxide fluid technology

To discuses and investigate the electrical, physical, and ferroelectric properties of as-deposited thin films, the supercritical carbon dioxide fluid (SCF) process were used by a low temperature treatment. The ferroelectric thin films were post-treated by SCF process which mixed with propyl alcohol and pure H_2O. After SCF process treatment, the remnant and saturation polarization increased in hysteresis curves, and the passivation of oxygen vacancy and defect in leakage current density curves were found. Besides, the qualities of as-deposited ferroelectric thin films using SCF process treatment were carried out XPS, C-V, and J-E results.

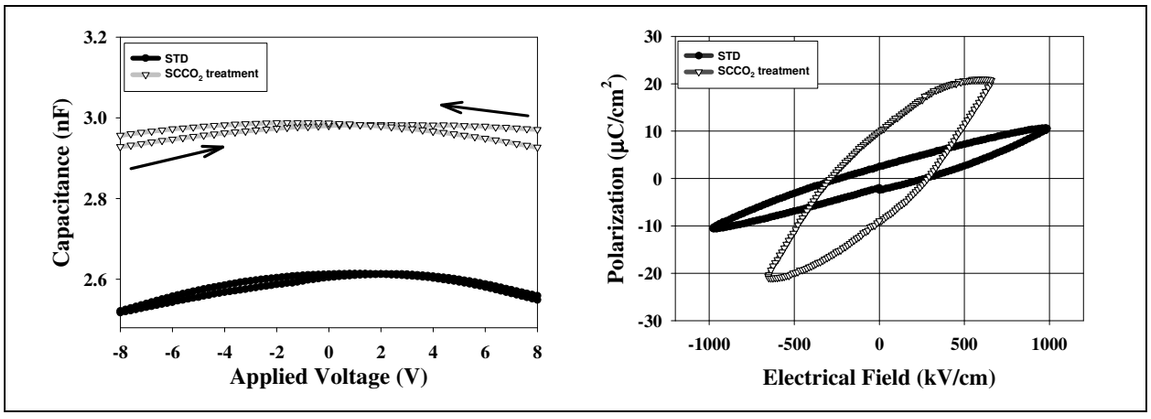

Fig. 11. (a) The C-E characteristics of as-deposited and $SCCO_2$-treated BZ1T9 thin films, and (b) The J-E characteristics of as-deposited and $SCCO_2$-treated BZ1T9 thin films.

Figure 11(a) compares the change in the capacitance versus the applied voltage (C-V) for the non-treatment and $SCCO_2$ fluid treatment BZ1T9 thin films. The applied bias voltage ranges from -20 to 20 V. The capacitances of the BZ1T9 thin films appear to increase due to the $SCCO_2$ fluid treatment. The capacitances increase from 2.65 to 2.95 nF were found after the post-treatment. As suggested by the XPS analysis result, the improvement in the capacitance of the BZ1T9 thin films were attributed to the compensation of the oxygen vacancy of the ABO_3 phase in the BZ1T9 thin films.

Figure 11(b) shows the P-E curves of the thin films observed at a frequency of 500 kHz under a 20V applied voltage from the Sawyer-Tower circuits. After $SCCO_2$ fluid treatment, the 2Pr value and coercive filed of BZ1T9 thin films for MIM structure were about 20 $\mu C/cm^2$ and 250kV/cm, respectively. We found that remnant polarization were improved and increased from 3 to 10 $\mu C/cm^2$.

Figure 12(a) shows the wide-scan XPS spectrum of the BZ1T9 thin film in the binding energy range from 200 to 900 eV. From the spectrum it is clear that the BZ1T9 film contains Ba, Zr, Ti, and O elements near its surface, and no other impurity element was detected in the spectrum up to 900 eV. Quantitative XPS analysis result not only provides the chemical composition near the sample surface, but also gives the formation on the chemical bonding. From the spectrum of the chemical bonding observed, the compounds of the surface for BZ1T9 thin films would be determined. In addition, the narrow-scan XPS spectra of O 1s peaks for the BZ1T9 thin film were shown in Fig. 12(b).

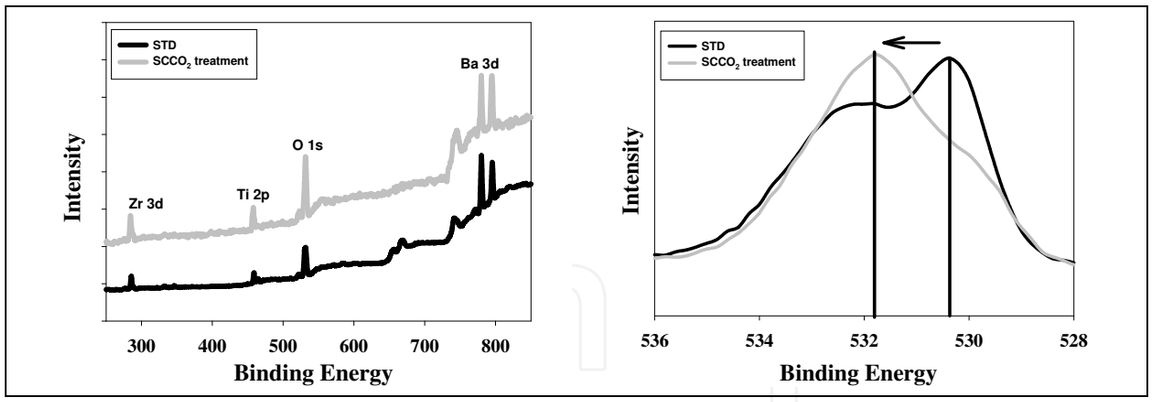

Fig. 12. (a)Wide-scan XPS spectrum and (b) O 1s energy levels of ferroelectric thin film after $SCCO_2$ fluid treatment.

To infer the variation in chemical bonding of BZ1T9 thin films during processing with $SCCO_2$ fluid treatment, a doublet structure was observed in the XPS spectrum of O 1s peak were found. Its component peak in the spectrum was fitted to a Guassian type distribution with lower binding energy (LBE) and higher binding energy (HBE) peaks at 529.62 eV and 531.68 eV, respectively. The LBE peak was due to the oxide and the HBE peak was due to the hydroxide/absorbed oxygen. These results induced that indicating that the H_2O molecules indeed can operatively react with the thin films dangling bonds (or traps) and form the stronger O 1s bonding.

2.3 Fabrication ferroelectric random access memory device on bottom-gated amorphous silicon thin-film transistors

Recently, the ferroelectric BZ1T9 composition was used in a one-transistor-capacitor (1TC) structure of the amorphous-Si TFT device to replace the gate oxide of random access memory devices. For that, a bottom-gate amorphous thin-film transistor, as shown in Fig. 13, was fabricated and the characteristics of the fabricated devices were developed.

The counter clockwise current hysteresis and memory window of n-channel thin-film transistor property were observed, and that were be used to indicate the switching of ferroelectric polarization of BZ1T9 thin films. Additionally, the ferroelectric random access memory device using bottom-gate amorphous silicon thin-film transistor with channel width=40 μm and channel length=8 μm has been successfully fabricated and the I_D-V_G transfer characteristics were also investigated.

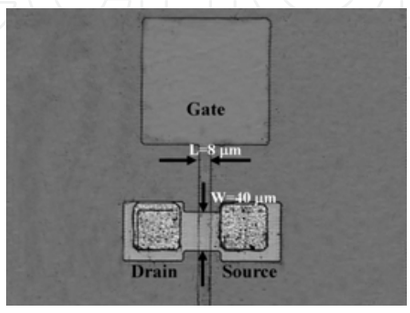

Fig. 13. The top view of the 1TC FeRAM device fabricated with BZ1T9 as the bottom-gate oxide.

After the optimum characteristics of BZ1T9 thin films were deposited, then the BZ1T9 thin films obtained at the optimum parameters were used to fabricate the one-transistor-capacitor (1TC) structure of the amorphous-Si TFT device, and the top view of the fabricated 1TC FeRAM device with BZ1T9 gate oxide was shown. The measured transfer characteristics of drain current and gate voltage (I_D-V_G) of the fabricated ferroelectric gate oxide 1TC FeRAM device were shown in Fig. 14. The a-Si TFT device using BZ1T9 gate oxide measured from the -5 to 20 V and then from 20 return to -5 V at drain voltage from 0.1 to 5V.

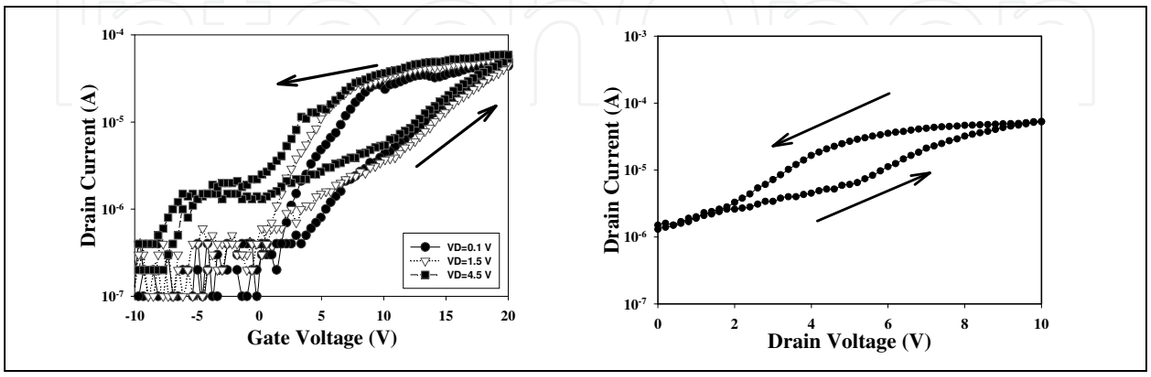

Fig. 14. I_D-V_G transfer characteristics of the fabricated 1TC FeRAM devices.

The counterclockwise current hysteresis and memory window of n-channel thin-film transistor property as indicated by arrows were observed, and the I_D-V_G transfer characteristics were used to indicate the switching of ferroelectric polarization of BZ1T9 thin films. From the measured results, the drain current is less than 1×10^{-7}A around V_G=-1V and larger drain current of 4×10^{-5}A as V_G=10V were found. It was interesting to note that the memory windows are 12 and 20V, respectively, when the drain voltages are increased from 0.1 to 5V. As Fig. 14 shows, the threshold voltage and sub-threshold characteristics were obtained, and threshold voltage was about -4V. Besides, the on/off drain current ratio was about the magnification of two orders. The on/off current ratio obtained from the fabricated 1TC FeRAM device in this study was much smaller than that of the most reported bottom-gated TFTs devices by using different ferroelectric materials as gate oxide.
Figure. 14 shows the measured drain current versus drain voltage (I_D–V_D) characteristics of 1TC FeRAM devices with a channel length of 30 μm. The 1TC FeRAM device has properties typical of n-channel transistors and exhibits clear current saturation. In addition, the (I_D–V_D) current window was found at V_G = 10 V. This was because the ferroelectric gate insulator can induce a considerably large charge. As shown in Fig. 14, we obtained an on-current of 5×10^{-5} A for the 1TC FeRAM devices with a channel length of 30 μm.

3. Conclusion

The post-treatment technology, such as CTA, RTA, $SCCO_2$ and oxygen plasma treatment was an effective method to remove the vacancies and defects for as-deposited ferroelectric thin films. The post-treatment technology was developed to take the oxygen molecules to terminate the traps for as-deposited thin films. The improvement effect in the leakage current mechanism of the as-deposited thin film using post-treatment technology was discussed. The capacitance increased for reduction of interface states and passivation of traps in the as-deposited thin films treated by post-treatment technology was observed.

Besides, the one-transistor-capacitor (1TC) structure of ferroelectric random access memory (FeRAM) with the gate oxide of BZ1T9 thin films on the amorphous-Si TFT structure were investigated and fabricated. The on/off drain current ratio was two orders (10^2), and the value was much smaller than those of the most reported bottom-gated TFTs devices by using different ferroelectric materials as gate oxide. From these results in our study, the BZ1T9 thin film for bottom-gate amorphous-Si thin-film transistor was an excellent candidate to fabricate higher storage capacitance ferroelectric random access memory devices.

4. Acknowledgment

The authors will acknowledge to Prof. Ting-Chang Chang and Prof. Cheng-Fu Yang. Additionally, this work will acknowledge the financial support of the National Science Council of the Republic of China (NSC 99-2221-E-272-003) and (NSC 97-2221-E-272-001).

5. References

[1] J. M. Kim, D. S. Yoon, and K. No: J. Mater. Sci. 29 (1994) 6599.
[2] S. Y. Wu: IEEE Trans. Electron Devices 21 (1974) 499.
[3] S. Y. Wu: Ferroelectrics 11 (1976) 379.
[4] H. Buhay, S. Sinharoy, W. H. Kasner, M. H. Francombe, D. R. Lampe, and E. Stepke: Appl. Phys. Lett. 58 (1991) 1470.
[5] P. T. Liu, Y. T. Chou, L. F. Teng, F. H. Li, H. P. Shieh: Appl. Phys. Lett. 98 (2011) 052102.
[6] J. S. Park, T. S. Kim, K. S. Son, W. J. Maeng, H. S. Kim, M. Ryu, and S.g Y. Lee: Appl. Phys. Lett. 98 (2011) 012107.
[7] M. Kimura, T. Kamiya, T. Nakanishi, K. Nomura, and H. Hosono: Appl. Phys. Lett. 96 (2010) 262105.
[8] K. Sugibuchi, Y. Kurogi and N. Endo: J. Appl. Phys., 46 (1975) 2877.
[9] I. G. Ismailzade, V. I. Nesterenko, Sov. Phys. Crystallogr. 12 (1968) 625.
[10] M. Kimura, T. Sawada, A. Ando, Y. Sakabe, Jpn, J. Appl. Phys. 38 (1998) 5557.
[11] J. F. Scott and C. A. Paz de Araujo, Science 246, 1400 (1989).
[12] D. J. Taylor, R. E. Jones, P. Zurcher, P. Chu, Y. T. Lii, B. Jiang, and S. J. Gillespie, Appl. Phys. Lett. 68, 2300 (1996).
[13] J. F. Scott and C. A. Paz de Araujo, Science 246, 1400 (1989).
[14] C. A. Araujo, J. D. Cuchiaro, L. D. McMillian, M. C. Scott, and J. F. Scott, Nature (London) 374, 627 (1995).
[15] B. H. Park, B. S. Kang, S. D. Bu, T. W. Noh, J. Lee, and W. Jo, Nature (London) 401, 682 (1999).
[16] C. C. Leu, L. R. Yao, C. P. Hsu, and C. T. Hu, J. Electrochem. Soc., 157, 3, (2010) G85.
[17] K. H. Chen, Y. C. Chen, C. F. Yang, and T. C. Chang, J. Phys. Chem. Solids, vol. 69, (2008) 461.
[18] C. F. Yang, K. H. Chen, Y. C. Chen, and T. C. Chang, IEEE Trans. Ultrason. Ferroelectr. Freq. Control, 54 (2007) 1726.
[19] C. F. Yang, K. H. Chen, Y. C. Chen, and T. C. Chang, Appl. Phys. A, 90 (2008) 329.
[20] K. H. Chen, Y. C. Chen, Z. S. Chen, C. F. Yang, and T. C. Chang, Appl. Phys. A, 89 (2007) 533.
[21] G. Velu, C. Legrand, O. Tharaud, A. Chapoton, D. Remiens, and G. Horowitz, Appl. Phys. Lett. 79 (2001) 659.

[22] K. H. Chen, Y. C. Chen, C. F. Yang, and T. C. Chang: J. Phys. Chem. Solids 69 (2007) 461.
[23] K. H. Chen, C. F. Yang, C. H. Chang, Y. J. Lin : J. Jap. Appl. Phys., 48 (2009) 091401.
[24] J. Miao, J. Yuan, H. Wu, S. B. Yang, B. Xu, L. X. Cao, and B. R. Zhao, Appl. Phys. Lett. 90 (2001) 022903.
[25]C. F. Yang, K. H. Chen, Y. C. Chen, and T. C. Chang: Appl. Phys. A 90 (2008) 329.
[26] T. Kijima and H. Matsunaga, Jpn. J. Appl. Phys. 38, (1999) 2281.
[27] T. Watanabe, H. Funakubo, M. Osada, Y. Noguchi and M. Miyayama, Appl. Phys. Lett. 80, No.1 (2002).
[28] S. S. Kim, T. K. Song, J. K. Kim and J. Kim, J. Appl. Phys. 92, No.4 (2002)
[29] Y. Noguchi and M. Miyayama, Appl. Phys. Lett. 78, No.13 (2001).
[30] E. K. Choi, S. S. Kim, J. K. Kim, J. C. Bae, W. J. Kim, Y. I. Lee, T. K. Song, Jpn. J. Appl. Phys,Part 1. 43 (1) (2004) 237.
[31]B. H. Park, B. S. Kang, S. D. Bu, T. W. Noh, L. Lee, and W. Joe, Nature (London) 401, 682 (1999).
[32] Y. Noguchi, I. Miwa, Y. Goshima, and M. Miyayama, Jpn. J. Appl. Phys., Part 2 39, L1259 (2000).
[33] Y. Noguchi and M. Miyayama, Appl. Phys. Lett. 78, 1903 (2001).
[34] T. Friessnegg, S. Aggarwal, R. Ramesh, B. Nielsen, E. H. Poindexter, and D. J. Keeble, Appl. Phys. Lett. 77, 127 (2000).
[35] W. Takayuki, F. Hiroshi, O. Minoru, N. Yuji, M. Masaru, Appl. Phys. Lett. 80, (2002) 100.
[36] B. H. Park, B. S. Kang, S. D. Bu, T. W. Noh, L. Lee, and W. Joe, Nature (London) 401, (1999) 682.
[37] X. J. Meng, J. H. Ma, J. L. Sun, T. Yu, J. Lin, G. S. Wang, J. H. Chu, Appl. Phys. Lett. 78, (2004) 1089.
[38] B. H. Park, B. S. Kang, S. D. Bu, T. W. Noh, L. Lee, and W. Joe, Nature (London) 401, (1999) 682.
[39] Y. Noguchi, I. Miwa, Y. Gosima, and M. Miyayama, Jpn. J. Appl. Phys., Part 2 39, (2000) L1259.
[40] Y. Noguchi and M. Miyayama, Appl. Phys. Lett. 78 (2001) 1903.
[41] T. Friessnegg, S. Aggarwal, R. Ramesh, B. Nielsen, E. H. Poindexter, Jpn. J. Appl. Phys., Part 1 40 (2001) 5572.
[42] P. Orgiani, R. Ciancio, A. Galdi, S. Amoruso, and L. Maritato, Appl. Phys. Lett. 96 (2010) 032501.
[43] W. Lim, E. A. Douglas, D. P. Norton, S. J. Pearton, F. Ren, Y. W. Heo, S. Y. Son, and J. H. Yuh, Appl. Phys. Lett. 96, (2010) 053510.
[44] D. Y. Wang, S. Li, H. L. W. Chan, and C. L. Choy, Appl. Phys. Lett. 96, (2010) 061905.
[45] C. C. Lin and C. C. Lee, J. Electrochem. Soc., 157, 2, (2010) A230.
[46] K. Tajima, Y. Yamada, S. Bao, M. Okada, and K. Yoshimura, J. Electrochem. Soc., 157, 3, (2010) J92.
[47] N. C. Su, S. J. Wang, and Albert Chin, Electrochem. Solid-State Lett., 13, 1, (2010) H8.
[48] O. Tuna, Y. Selamet, G. Aygun and L. Ozyuzer, J. Phys. D, 43 (2010) 055402.
[49] K. F. Chiu, C. C. Chen, M. H. Chiang, and W. H. Ho, J. Electrochem. Soc., 157, 2, (2010) A130.
[50] C. C. Chen, K. F. Chiu, K. M. Lin, H. C. Lin, C. R. Yang, F. M. Wang, and M. H. Chiang, J. Electrochem. Soc., 157, 3, (2010) A289.
[51] M. Furuta, T. Nakanishi, M. Kimura, T. Hiramatsu, T. Matsuda, H. Furuta, T. Kawaharamura, C. Li, and T. Hirao, Electrochem. Solid-State Lett., 13, 4, (2010) H101.

[52] S. J. Won, S. S. Sang, W. Lee, G. J. Choi, C. S. Hwang, and H. J. Kim, Electrochem. Solid-State Lett., 13, 2, (2010) G13.
[53] C. L. Sun, P. C. Juan, Y. W. Hsu and Y. W. Liu, Thin Solid Films, 518, 24, (2010) 7433.
[54]C. F. Yang, K. H. Chen, Y. C. Chen, and T. C. Chang, Appl. Phys. A, 90, 2, (2008) 329.
[55] A. D. Li, D. Wu, H. Q. Ling, M. Wang, Z. Liu and N. Ming, J. Cryst. Growth, 235 (2002) 394.
[56] V. R. Palkar, S. Chattopadhyay, S. C. Purandare, S. G. Lokhre, R. Pinto and M. S. Multani, Mater. Lett.33 (1997) 1.
[57] J. Li, L. Zhang, X. Yao and J. Wang, Ceram. Int., 30 (2004) 1509.
[58] M. L. Calzada, A. Gonzalez, R. Jimenez, C. Alemany and J. Mendiola, J. Euro. Ceram. Soc. 21 (2001) 1517.
[59] Y. Wang, L. Li, J. Qi and Z. Gui, Ceram. Int. 28, 6 (2002) 657.
[60] K. H. Chen, Y. C. Chen, C. F. Yang, and T. C. Chang: J. Phys. Chem. Solids 69 (2007) 461.
[61] S. Fleischer, P. T. Lai, and Y. C. Cheng, J. Appl. Phys. 73 (1994) 8353.
[62] T. Mihara and H. Watanabe, Part I, Jpn. J. Appl. Phys. 34 (1995) 5664.
[63] Y. B. Lin and J. Y. Lee, J. Appl. Phys. 87 (2000) 1841.
[64] T. A. Rost, H. Lin and T. A. Rabson, Appl. Phys. Lett., 59 (1991) 3654.
[65] M. Yoshimoto, M. Anami, H. Shinohara, T. Yoshihara, H. Takagi, S. Nagao, S. Kayano and T.Nakano: IEEE Trans., Solid State Circuits, 18 (5) (1983) 479.
[66] T. Matsuda, K. Miyoshi, R. Yamaguchi, S. Moriya and T. Hosoya, K. Harada: IEEE Trans., Solid State Circuits, 20 (1) (1985) 88.
[67] J. Welser, S. Tiwari, S. Rishton, K. Lee and Y. Lee: IEEE Trans., Electron Device Lett., 18 (6)(1997) 278.
[68] N. Young, G. Harkin, R. Bunn, D. McCulloch and I. French: IEEE Trans., Electron Device,43 (11) (1991) 1930.
[69] S. Y. Wu: IEEE Trans., Electron Devices, (1974) 499.
[70] S. Y. Wu: Ferroelectr., 11 (1976) 379.
[71] H. Buhay, S. Sinharoy, W. H. Kasner, M. H. Francombe, D. R. Lampe and E. Stepke, Appl. Phys. Lett., 58 (1991) 1470.
[72] K. Sugibuchi, Y. Kurogi and N. Endo: J. Appl. Phys., 46 (1975) 2877.
[73] T. A. Rost, H. Lin, T. A. Rabson, R. C. Baumann and D. C. Callahan, IEEE Trans. Ultrason. Ferroelectr. Freq. Control, 38 (1991).
[74] S. R. Shannigrahi and H. M. Jang, Appl. Phys. Lett., 79 (2001)1051.
[75] S. K. Hong, C. W. Suh, C. G. Lee, S. W. Lee, E. Y. Hang and N. S. Kang: Appl. Phys. Lett., 77 (2000) 76.
[76] S. B. Xiong and S. Sakai: Appl. Phys. Lett., 75 (1999) 1613.
[77] J. S. Kim and S. G. Yoon: J. Vac. Soc. Technol., B 18 (1) (2000) 216.
[78] T. B. Wu, C. M. Wu and M. L. Chen: Appl. Phys. Lett., 69 (1996) 2659.
[79] M. She, H. Takeuchi and T. J. King: IEEE Trans., Electron Device Lett., 25 (5) (2003) 309.
[80] Y. K. Lee, J. S. Sim, S. K. Sung, C. J. Lee, T. H. Kim and J. D. Lee: IEEE Trans., Electron Device Lett., 23 (11) (2002) 664.
[81] M. W. J. Prins, K. O. Grosse-Holz, G. Muller, J. F. M. Cillessen, J. B. Giesbers, R. P. Weening and R. M. Wolf: Appl. Phys. Lett., 68 (1996) 3650.
[82] T. Miyasako, M. Senoo and E. Tokumitsu: Appl. Phys. Lett., 86 (2005).

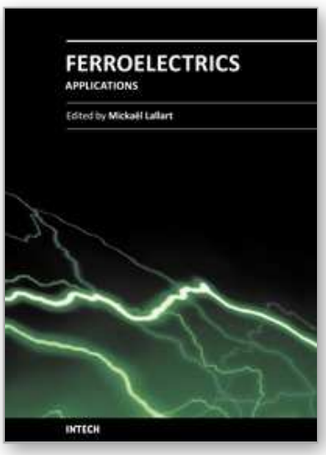

Ferroelectrics - Applications
Edited by Dr. MickaÃ«l Lallart

ISBN 978-953-307-456-6
Hard cover, 250 pages
Publisher InTech
Published online 23, August, 2011
Published in print edition August, 2011

Ferroelectric materials have been and still are widely used in many applications, that have moved from sonar towards breakthrough technologies such as memories or optical devices. This book is a part of a four volume collection (covering material aspects, physical effects, characterization and modeling, and applications) and focuses on the application of ferroelectric devices to innovative systems. In particular, the use of these materials as varying capacitors, gyroscope, acoustics sensors and actuators, microgenerators and memory devices will be exposed, providing an up-to-date review of recent scientific findings and recent advances in the field of ferroelectric devices.

InTech Europe
University Campus STeP Ri
Slavka Krautzeka 83/A
51000 Rijeka, Croatia
Phone: +385 (51) 770 447
Fax: +385 (51) 686 166
www.intechopen.com

InTech China
Unit 405, Office Block, Hotel Equatorial Shanghai
No.65, Yan An Road (West), Shanghai, 200040, China
中国上海市延安西路65号上海国际贵都大饭店办公楼405单元
Phone: +86-21-62489820
Fax: +86-21-62489821

IntechOpen